Rydberg Microwave-Frequency-Comb Spectrometer

Li-Hua Zhang,[1,2] Zong-Kai Liu,[1,2] Bang Liu,[1,2] Zheng-Yuan Zhang,[1,2] Guang-Can Guo,[1,2] Dong-Sheng Ding,[1,2,*] and Bao-Sen Shi[1,2,†]

[1] *Key Laboratory of Quantum Information, University of Science and Technology of China, Hefei, Anhui 230026, China*

[2] *Synergetic Innovation Center of Quantum Information and Quantum Physics, University of Science and Technology of China, Hefei, Anhui 230026, China*

(Received 8 October 2021; revised 5 May 2022; accepted 13 June 2022; published 14 July 2022)

The developing frequency-comb spectral technologies have potential applications and prospects in the wide fields of cosmology, meteorology, and microwave measurement. Here, we demonstrate a Rydberg microwave-frequency-comb spectrometer via multiple-microwave field dressing, providing precise microwave measurement. The Rydberg microwave-frequency-comb spectrum provides a real-time and absolute-frequency measurement with a range of 125 MHz and gives the relative phase of a single-frequency microwave signal. The reported experiment helps real-time sensing of an unknown microwave signal over a wide range using Rydberg atoms, which are vital for Rydberg-atom-based microwave metrology.

DOI: 10.1103/PhysRevApplied.18.014033

I. INTRODUCTION

A frequency comb consists of phase-stabilized narrow frequency lines with equidistant mode spacing (repetition frequency) [1]. Frequency-comb spectroscopy has found various applications in frequency, time, and distance measurement over the past decade and in precision spectroscopy [2] such as optical-frequency synthesis and frequency reference in optical atomic clocks [3,4]. There is much experimental progress on the excitation of frequency-comb spectroscopy in a variety of systems based on different physical mechanisms, such as a second-order Kerr optical-frequency comb in a microresonator [5,6], a broadband microwave- (MW) frequency comb via the nonlinear pumped cavity in a superconductor resonator [7] and a MW-frequency comb generated in a circuit QED device [8]. Other MW-frequency-comb-generation methods include semiconductor lasers with harmonic frequency locking [9,10] and optomechanical effects[11]. Frequency-comb spectroscopy with various systems and different bands such as the optical-frequency band and the MW-frequency band have distinct applications. For example, a MW-band frequency-comb spectrum could provide a method of directly measuring MW electric fields [2], detecting free radicals [12], and monitoring the intermediate products of a chemical reaction [13].

The exploration of state-of-the-art MW-frequency-comb (MFC) spectroscopy is important for such fields as timing, metrology, communications, and radio astronomy. MFC spectroscopy, with its wide range, low noise, and high stability, plays a crucial role in MW applications [2]. Compared with an optical-frequency comb, a MFC can have small mode spaces across its bandwidth owing to the lower carrier frequency. Because of the large transition dipole moment [14], the coupling between Rydberg atoms and the external MW electric fields is strong [15,16]. The development of a new type of Rydberg MFC spectrometer would have a distinct significance because Rydberg atoms, as a metrological resource, have potential advantages in amplitude [17–19], phase [20,21] sensing, channel capacity [22], and subwavelength imaging [23] and have a wide working bandwidth [24], and the Rydberg atomic sensor can be combined with deep-learning technology [25].

In this work, we theoretically and experimentally demonstrate a MW sensing protocol via a Rydberg MFC method in thermal cesium (Cs) atomic gas. Via multiple local MW fields, the excited Rydberg atoms are dressed and display comblike rf transitions. We show the proof-of-principle effectiveness of this spectral detection of the MW fields. A signal MW field with a maximum frequency range of ± 3.5 MHz is measured with a resolution of approximately 0.1 kHz: the amplitude and phase of the signal field are both retrieved and a measurement range of 125 MHz is demonstrated. The Rydberg MFC method does work for a MW signal with a certain spectral width. The demonstrated Rydberg MFC spectrometer may be a first step toward precise MW measurement using the atom-based MFC method.

*dds@ustc.edu.cn
†drshi@ustc.edu.cn

II. METHOD AND EXPERIMENT SETUP

The energy level is depicted in Fig. 1(a), and consists of a ground state $|g\rangle$ and two Rydberg states, $|r_1\rangle$ and $|r_2\rangle$. A laser resonantly couples the ground state $|g\rangle$ and the Rydberg state $|r_1\rangle$ with Rabi frequency Ω. A MFC field E_{MFC} and a signal field E_s, with Rabi frequencies $\sum_i \Omega_{\mathrm{LO_i}}$ and Ω_s, drive the Rydberg rf transitions $|r_1\rangle \leftrightarrow |r_2\rangle$. Then, these two MW fields are mixed via Rydberg atoms [19,20] through the interaction between the MW fields and Rydberg atoms, resulting in several beat notes between the signal and MFC comb lines, which are read from the transmission spectrum. This can be regarded as the beat effect of the transition probability [26]. As the frequency of the MW field is much higher compared with the difference-frequency component of the beat note, the sum-frequency component of the beat note is ignored, and the difference-frequency component is reserved. The strongest beat is the one between the signal and its nearest-neighbor MFC line. In addition, at least two MFCs with different mode spaces are used to obtain the absolute frequency of the signal, since the frequency of the beat note between one MFC field and the signal field only contains information on the relative frequency of the signal compared to its nearest-neighbor MFC comb line [27].

The total field in the atoms is written as [20]

$$\begin{aligned} E_{\mathrm{atom}} &= \sqrt{|E_L|^2 + |E_s|^2 + 2|E_L||E_s|\cos(\Delta\omega t + \Delta\phi)} \\ &\approx |E_L| + |E_s|\cos(\Delta\omega t + \Delta\phi). \end{aligned} \tag{1}$$

Here, the single local-oscillator (LO) field term E_{L} is replaced by a MFC field $E_{\mathrm{MFC}} = \sum_i E_{\mathrm{LO}_i}\cos(\omega_i t + \phi_i)$, in which $E_{\mathrm{LO}_i} = E_{\mathrm{LO}}$ corresponds to the strength of the ith frequency-comb line. Because of the limited bandwidth of the system [28], we set the MFC repetition rate f_r to be larger than the instantaneous bandwidth of the system. The field sensed by the Rydberg atoms can be expressed as

$$E_{\mathrm{atom}} \approx \sqrt{N_L}|E_{\mathrm{LO}}| + \frac{1}{\sqrt{N_L}}|E_s|\cos(\Delta\omega_k t + \Delta\phi_k), \tag{2}$$

where N_L represents the number of MFC comb lines. The subscript k represents the number of the MFC line nearest to the signal field. When $E_s \ll E_{\mathrm{LO}}$, the beat term between MFC comb lines, $2|E_{\mathrm{LO}_{i,i\neq k}}||E_s|\cos(\Delta\omega_i t + \Delta\phi_i)$, is small compared with the square of the LO electric field strength $|E_{\mathrm{LO}}|^2$. According to Eq. (2), the signal amplitude and phase are extracted from its beat note with the nearest-neighbor MFC comb line. As shown in Fig. 1(b), two MFCs are used (denoted as E_{MFC_1} and E_{MFC_2}) to measure the absolute frequency of the signal field E_s. For a proof-of-principle study, we turn on one of the MFCs at a different time. We set these two MFCs with the same offset frequency f_{offset} and with different repetition rates. The difference between the repetition rates is marked as δf_r and it satisfies $\delta f_r = f_r - f_{r'} \ll f_r$. The exact-fraction method in Ref. [27] is employed to calculate the frequency of the signal f_s, as follows:

$$f_s = f_{\mathrm{offset}} + Nf_r \pm f_b. \tag{3}$$

The mode-order number of the signal is calculated according to the sum or difference of the two beat-note frequencies $f_b, f_{b'}$. The mode-order number for the MFC1 and MFC2 is marked as N_1 and N_2 (start from 0). Also, the two MFCs both have N_c comb lines. Let us assume that the repetition rates satisfy $f_r > f_{r'}$. The calculation of the mode-order number N is divided into two cases:

Case 1. $N_2 - N_1 = 1$. When $f_r - (f_b + f_b') \leq (N_c - 2)\,\delta f_r$, the mode-order number of MFC2 is $(f_r - f_b - f_b')/\delta f_r$-1.

Case 2. $N_1 = N_2$. If the condition in case 1 is not satisfied, the mode-order number of MFC2 is given by $N_2 = (f_b + f_b')/\delta f_r$ or $N_2 = (|f_b - f_b'|)/\delta f_r$. And if $f_b + f_b' > N_c$, $N_2 = (|f_b - f_b'|)/\delta f_r$.

The calculation of the mode-order number with part of the experimental data measured in Fig. 2(b) is given in Table I. Finally, the signal frequency can be calculated by means of Eq. (3).

The mode-order number N is often not an integer because of the finite measurement precision of the beat frequencies f_b and $f_{b'}$. To correctly estimate N, the resolution bandwidth of the data-acquisition device (e.g., the resolution bandwidth of a spectrum analyzer) should be set larger than δf_r. The value δf_r satisfies the formula $N\delta f_r < f_r/2$. This guarantees that the mode-order numbers of the signal with combs 1 and 2 have a difference less than 1. As the beat note with the nearest-neighbor comb line is the strongest one within a range of $f_r/2$, we only monitor the signal in this range. As a proof-of-principle experiment, we turn on the two MFCs at different times and keep the amplitude of the signal unchanged to demonstrate the frequency measurement. (In practice, the use of two vapor cells applied with two different MFCs could be an effective method for real-time frequency measurement.)

We use three infrared lasers [29,30] to excite the Cs atoms from the ground state $|g\rangle$ to the Rydberg state $|r_1\rangle$. The laser beams consist of probe, dressing, and coupling lasers. The probe laser is resonant with the transition $6S_{1/2}, F = 4 \rightarrow 6P_{3/2}, F' = 5(|1\rangle \rightarrow |2\rangle)$ and the dressing laser couples the transition $6P_{3/2}, F' = 5 \rightarrow 7S_{1/2}, F'' = 4$ $(|2\rangle \rightarrow |3\rangle)$ through the two-photon spectrum. The probe beam is split into two beams and is collected by a balanced photodetector. Both the coupling and the dressing beams counterpropagate with the probe beam. We use a differential detection scheme to measure the transmission

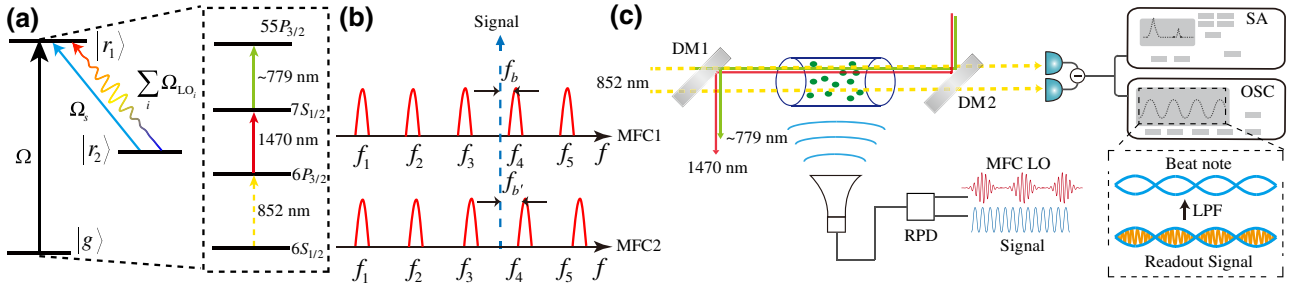

FIG. 1. (a) The energy diagram of a Rydberg MFC spectrum. A laser drives the ground state $|g\rangle$ and the Rydberg state $|r_1\rangle$. For the experiment, three lasers are used to excite the atoms, as shown in the dashed box. A strong MFC field is set as a local oscillator (LO) field (multicolor) and a signal field (blue) couples the two Rydberg states $|r_1\rangle$ and $|r_2\rangle$. (b) The signal beat (blue) with two MFCs (red). The beat-note frequencies are determined by the frequencies of the signal field and its nearest-neighbor MFC comb line. From the sum and difference of the $f_b \pm f_{b'}$, we calculate the mode-order number N of the nearest-neighbor MFC comb line. The absolute frequency of the signal field is obtained from the mode-order number and its offset from its nearest MFC frequency component. (c) The experimental setup. A 852-nm probe laser, a 1470-nm dressing laser, and a 779-nm coupling laser are used to excite and probe the Rydberg state. The MFC and signal fields are combined through a resistance power divider (RPD) and transmitted to the vapor cell by a horn antenna. The beat-note signal is recorded and analyzed via an oscilloscope (OSC) or a spectrum analyzer (SA).

spectrum. The MFC and signal fields interact with the Rydberg atoms simultaneously and the transmission spectrum displays an interference beating via the mixing process in the Rydberg atoms. This beat note is extracted from the transmission spectra via a low-pass filter [Fig. 1(c)]. We use a spectrum analyzer to collect the frequency and amplitude of this signal.

III. PERFORMANCE FOR FREQUENCY MEASUREMENT

To demonstrate the wide response range of the Rydberg MFC spectrometer, we measure the amplitude of the output beat note versus the signal-field frequency f_s. By fixing the power of the signal MW field to approximately -30 dBm, we change the frequency offset of the signal δf with respect to the Rydberg rf transition $55P_{3/2} \longleftrightarrow 54D_{5/2}$ (with 4.485 GHz) from -18 MHz to $+18$ MHz. The amplitude of the output beat note is shown in Fig. 2(a). There are nine peaks, which correspond to the number of applied MFC comb lines. Each peak reflects the beat-note response between the individual comb-line component and the signal. The peak profile is related to the finite instantaneous band of the system (the 3-dB instantaneous band δw is 300 kHz for our system), which is determined by the time for the system to reach the steady state [28]. This finite band can be described by optical Bloch equations, which should consider the time-dependent response of the atomic system (see the further analysis and estimation of the instantaneous bandwidth in Appendixes B and C). The black solid curve in Fig. 2(a) shows the theoretical result, which is normalized to the maximum amplitude of the signal at each peak. The instantaneous bandwidth δw is small compared with half of the repetition rate f_r of the MFC, e.g., 2 MHz, and the observed power of the beat note decreases rapidly when the frequency of the signal gets away from its nearest-neighbor MFC comb line. Furthermore, the maximum response appears when the signal is close to the MFC comb line. With increasing signal frequency offset δf from the resonance, the beat-note response is reduced. The theoretical calculation is the red dashed line. This is modeled by numerically solving the semisteady state of the master equation. The response when applying a MFC with 25 comb lines is illustrated in Fig. 6 of Appendix A to show the maximum response of the system.

In Fig. 2(b), we show the retrieved frequency versus the signal frequency when two MFCs (25 comb lines) covering a range of approximately 7 MHz are applied. The repetition rates of these two MFCs, f_r and $f_{r'}$, are 280 kHz and 279 kHz, respectively. The difference in the repetition rate is $\delta f_r = f_r - f_{r'} = 1$ kHz. We set the resolution bandwidth of the spectrum analyzer, Δ_{RBW}, as 30 Hz (less than δf_r) to extract the mode-order number N. Thus, the deviation between the input and the retrieved signal is determined by the resolution of the measurement device, as shown in Fig. 2(b). In our experiment, the resolution bandwidth of the spectrum analyzer, Δ_{RBW}, is set as 10 Hz. This protocol has advantages over the method of scanning the frequency of a single LO field [19], since there is no extra requirement to adjust the LO frequency to capture the signal in the limited bandwidth. This realizes real-time signal detection over a wide range.

IV. RECEIVING A 1-kHz-BANDWIDTH SIGNAL

In practice, the input MW field often has a certain bandwidth and different central frequencies, such as the MW field emitted from free radicals [12]. We demonstrate the

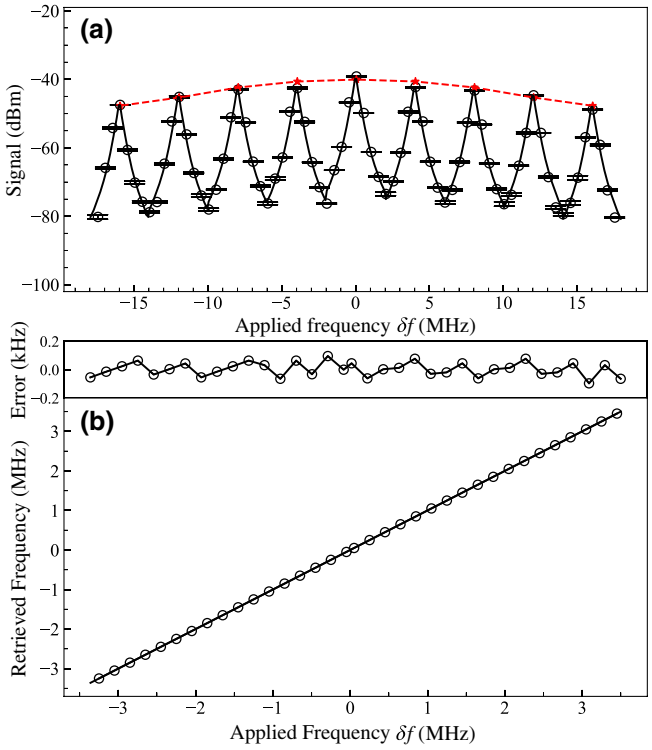

FIG. 2. (a) The power of the beat note versus the signal-field frequency offset δf . The experimental data (black circles), the semi-steady-state theoretical result (red dashed line), and the time-dependent calculation results (black solid line) are shown. The beat note is recorded with a frequency separation of 500 kHz. Here, a nine-bin MFC field is used. (b) The retrieved frequency versus the signal-field frequency. Here, two 25-bin MFCs are used. The inset at the top shows the frequency error of approximately 100 Hz.

ability of the system to measure the frequency of this kind of signal. In Fig. 3(a), the signal frequency spectrum received by different comb bins is shown. The input signal frequency spectrum and the output beat-note frequency spectrum are shown in Fig. 3(b), in which the selected different principal quantum numbers n are used to detect different frequencies. As a guide for the eye, the powers of the input signal are all shifted by -10 dBm and the profiles of the output signal are in good agreement with those of the input signal. The absolute frequency of the input signal is calculated through the frequency difference of the beat note. In this process, the bandwidth of the signal (1 kHz) is less than the repetition rate of the MFC.

V. PHASE RECOGNITION

The MFC sensing method allows recognition of the signal phase. We measure the output phase by changing the phase of the input signal field. The phase information is extracted from the sinusoidal fit coefficient in the formula $y = A\sin(\omega t + \phi)$. We set the MFC field with three comb lines and a frequency repetition rate of 300 kHz and set the signal frequency offset f_r at 300.05 kHz. The output phase versus the input signal phase is shown in Fig. 4. The inset of Fig. 4 corresponds to the transmission signal with an input phase of $\pi/6, \pi/2, 5\pi/6$, which shows that the transmission signal is phase sensitive to the input signal. The linear regression coefficient is 0.98 for the input and output phases. The reduced chi-square for this regression is 0.63, showing a linear dependency function, in which the small phase error is due to the fluctuation of the system.

VI. DISCUSSION

Compared with the heterodyne method [19] of addressing a single LO field, the demonstrated MFC method can measure the absolute frequency of a signal. This could promote applications in radar and communications because the heterodyne method can only detect the offset of the signal frequency $|\delta f|$ and has difficultly distinguishing the sign of the frequency, which reveals the direction of motion of an object. As limited by the evolution time to reach the steady state, the instantaneous bandwidth of the Rydberg MW sensor is typically less than 10 MHz in the traditional methods [28], while the MFC method can have an instantaneous working bandwidth of hundreds of megahertz considering the strong off-resonant response of the Rydberg atoms [24]. In addition, we consider the master equation as a simple way of describing the results. Since the MFC fields consist of multiple frequency lines, a more precise method such as a Floquet calculation would be more effective.

The MFC spectrometer based on Rydberg atoms has many potential advantages. For example, (1) there is no need to change the size of the Rydberg receiver, as the classical antenna should have its size changed to match MW electric fields with different frequencies, and (2) Rydberg atoms could be used to achieve high sensitivity via the mixing method [19]. A series of optimized operations that could improve the performance of this Rydberg MFC spectrometer include locking the lasers to an ultrastable cavity,

TABLE I. The mode-order number calculation.

	Case 1 ($N_1 - N_2 = 1$)	Case 2 ($N_1 = N_2$)
Beat-1 frequency, f_b	132.104 kHz	62.92 kHz
Beat-2 frequency, f_b'	130.019 kHz	49.955 kHz
Mode-order number	$N_2 = \left(280 - f_b - f_b'\right)/1 - 1 = 16.877 \approx 17$	$N_2 = (f_b - f_b')/1 = 12.965 \approx 13$

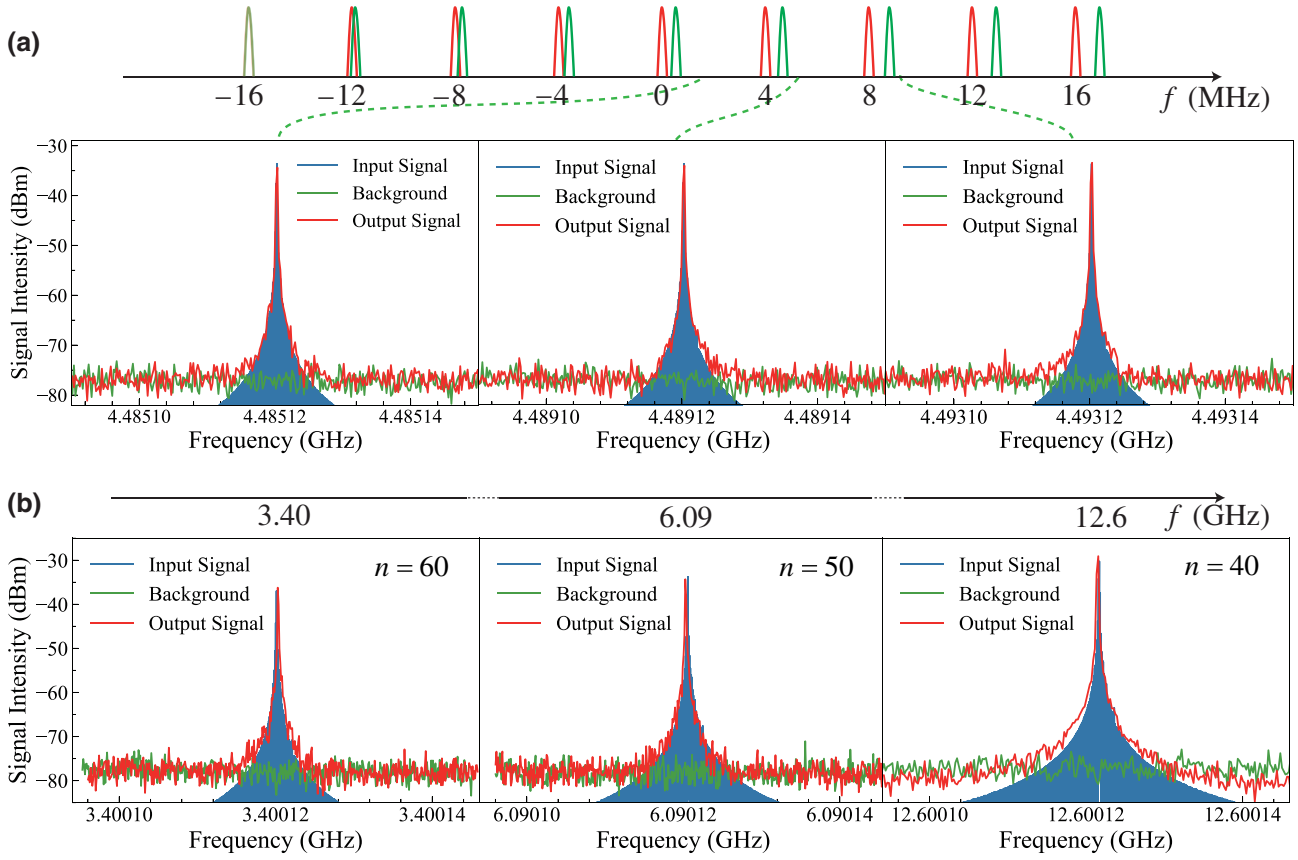

FIG. 3. (a) The received 1-kHz bandwidth signal spectrum near different comb bins. (b) The measured frequency spectrum for a signal with 1 kHz bandwidth: the amplitude of the frequency spectrum of the output beat notes using MFCs with central frequencies of 3.40 GHz, 6.09 GHz, and 12.6 GHz. The Rydberg states used are $60P_{3/2}$, $50P_{3/2}$, and $40P_{3/2}$, respectively.

reducing the system noise by using homodyne detection, and reducing the coupling loss of the MW electric fields by a waveguide [24].

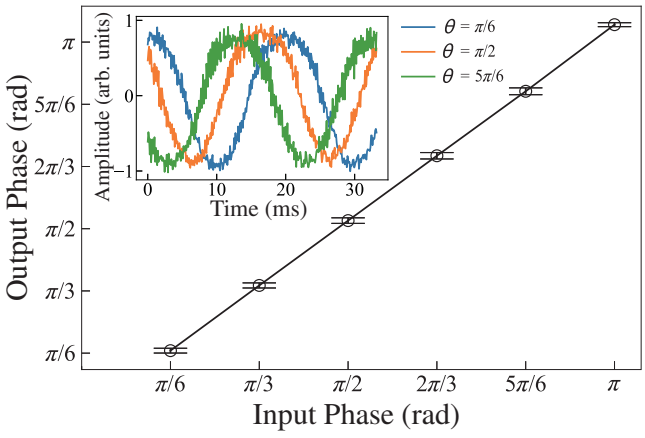

FIG. 4. The output phase versus the input phase. The inset is the recorded transmission signal. The extra noise in the transmission signal is mainly from the beat notes between the different MFC comb lines. The power of the signal field is −20 dBm.

VII. CONCLUSIONS

In summary, we demonstrate an absolute-frequency measurement through a Rydberg MFC spectrometer. The instant detection range can be further increased by improving the MFC bandwidth, so there is still room for improvement. The high-resolution spectroscopy of the Rydberg atoms allows precise detection of the electric fields and the Rydberg state [31,32]. Further study on various MW dressing protocols may improve the sensitivity, bandwidth, and precision in Rydberg atomic sensing [19,33,34]. Rydberg atoms also possess high sensitivity in the terahertz frequency range [35,36]. Thus, the combination of Rydberg atoms with a terahertz frequency comb [37,38] also permits precise, real-time, and coherent measurement of terahertz signals in communication and metrology.

ACKNOWLEDGMENTS

We acknowledge funding from the National Key R&D Program of China (Grant No. 2017YFA0304800), the National Natural Science Foundation of China (Grants No. U20A20218, No. 61525504, and No. 61435011), the Youth Innovation Promotion Association of the Chinese

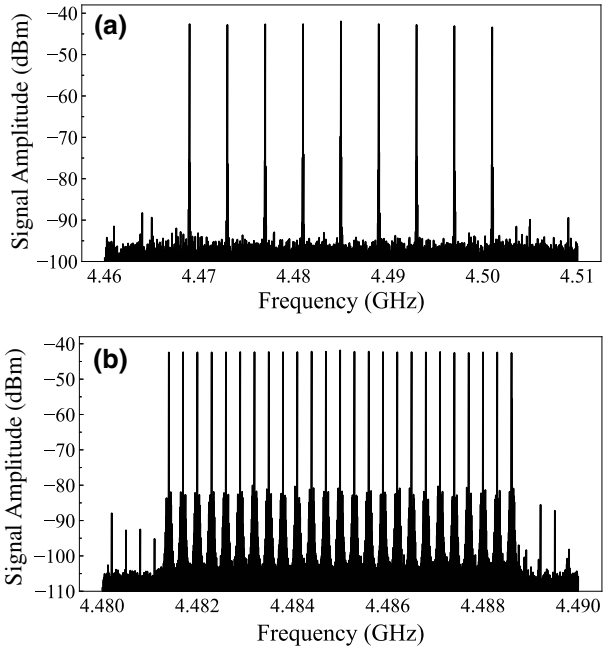

FIG. 5. Plots of the frequency spectra of the MFCs used in Fig. 2. (a) The frequency spectrum of the MFC used in Fig. 2(a). (b) The frequency spectrum for one of the MFCs used in Fig. 2(b).

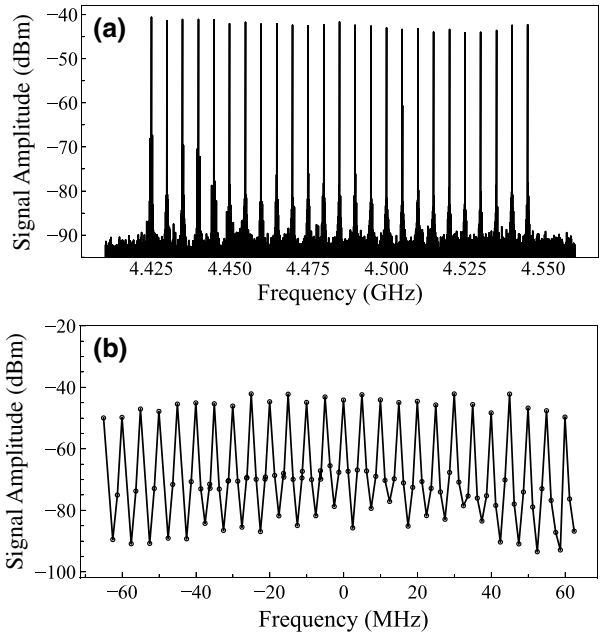

FIG. 6. (a) The spectrum of the MFC used to demonstrate the system maximum response range (125 MHz). (b) The power of the beat-note response versus the signal frequency when applying the MFC covering range of 125 MHz. Here, we set the signals with a constant power of approximately −20 dBm.

Academy of Sciences (Grant No. 2018490), and the Major Science and Technology Projects in Anhui Province (Grant No. 202203a13010001).

APPENDIX A: MFCS SETUP

As we know, a frequency comb consists of phase-stabilized narrow frequency lines with equidistant mode spacing (repetition frequency). Here, we use the multi-tone modulation of the vector signal generator (1465V Ceyear) to simulate a MFC signal. The central frequency of each MFC used in our experiment is set near 4.485 GHz to maximize the beat-note response to the signal field. The repetition rates of the MFC used in Figs. 2(a) and 2(b) are 4 MHz and 280 kHz, respectively. The frequency spectrum of the MFC used in our experiment is acquired through the spectrum analyzer (4024F Ceyear). The MFC frequency spectra are shown in Fig. 5. In the MFC frequency spectra, the main comb-line components dominate, so the effects of other comb-line components are weak. Besides, in Fig. 6(b), we also plot the power of the output beat note versus the applied signal frequency when a MFC with a range of 125 MHz is applied. Finally, the maximum comb span of the MFC is limited by the maximum clock frequency of the signal generator (about 125 MHz). Other MFC-generation methods can overcome this limitation to achieve a wider measurement range.

APPENDIX B: INSTANTANEOUS BANDWIDTH

The instantaneous bandwidth in this Rydberg atom-based MW receiving system refers to the first frequency of the (beat-note power) response reaching 50% (−3 dB) of its maximum value. We record the system response power versus the frequency of the beat note to measure this bandwidth. The frequency response of the MFC scheme is

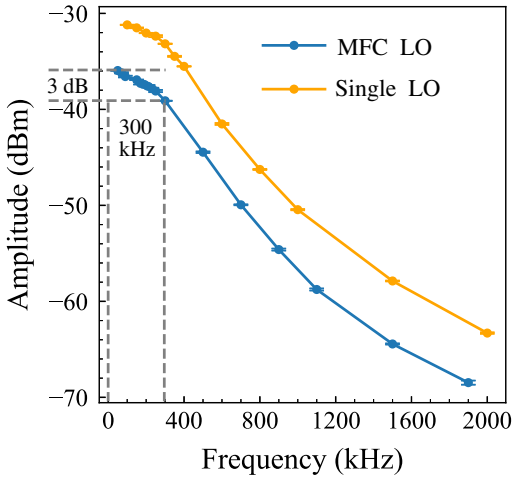

FIG. 7. The power of the beat note as a function of its frequency. The 3-dB instantaneous bandwidth is about 300 kHz and is indicated by the dashed line.

measured within a span of the MFC repetition rate, so the signal MW field only beats with one of the MFC comb lines. In Fig. 7, the instantaneous bandwidths are almost the same for the MFC LO and the single LO scheme, and the frequency response character (the profile of the response curve) is similar. This bandwidth is dependent on the relaxation time for the atoms to reach a steady state. For our experiment system, it is about 300 kHz. In the rubidium Rydberg-atom system, the bandwidth is several megahertz [20], which would be more helpful to achieve a flat beat-note response.

APPENDIX C: THEORETICAL CALCULATION

The dynamics of this system are described using the Lindblad equation [19,30]

$$\dot{\hat{\rho}} = \frac{i}{\hbar}[\hat{\rho}, \hat{H}] + L(\hat{\rho}). \tag{C1}$$

There are two regimes of beat-note response in Fig. 2(a): (i) When the beat-note frequency f_b (e.g., 50 kHz) is less than the instant bandwidth of the system (approximately 300 kHz), the power of the beat note is calculated through solving the steady-state Lindblad equation, which corresponds to the maximum signal at the top of each peak (red) in Fig. 2(a); (ii) When $f_b > 300$ kHz, we model the beat-note power reduction compared with its maximum value by a time-dependent optical Bloch equation and the numerical results are shown using solid lines in Fig. 2(a).

For the case $f_b < 300$ kHz, the system Hamiltonian under the bare-atom basis $|1\rangle$, $|2\rangle$, $|3\rangle$, $|4\rangle$, and $|5\rangle$ is

$$\hat{H} = \begin{pmatrix} 0 & \Omega_p/2 & 0 & 0 & 0 \\ \Omega_p/2 & \Delta_1 & \Omega_d/2 & 0 & 0 \\ 0 & \Omega_d/2 & \Delta_2 & \Omega_c/2 & 0 \\ 0 & 0 & \Omega_c/2 & \Delta_3 & \Omega_{\mathrm{MW}}(t)/2 \\ 0 & 0 & 0 & \Omega_{\mathrm{MW}}(t)/2 & \Delta_4 \end{pmatrix} \tag{C2}$$

and the Lindblad term in the above Eq. (C1) is

$$L(\hat{\rho}) = \begin{pmatrix} \Gamma_e\rho_{22} & -\frac{1}{2}\Gamma_e\rho_{12} & -\frac{1}{2}\Gamma_d\rho_{13} & -\frac{1}{2}\Gamma_{r1}\rho_{14} & -\frac{1}{2}\Gamma_{r2}\rho_{15} \\ -\frac{1}{2}\Gamma_e\rho_{21} & -\Gamma_e\rho_{22} + \Gamma_d\rho_{33} + \Gamma_{r2}\rho_{55} & -\frac{1}{2}(\Gamma_e + \Gamma_d)\rho_{23} & -\frac{1}{2}(\Gamma_e + \Gamma_{r1})\rho_{24} & -\frac{1}{2}(\Gamma_e + \Gamma_{r2})\rho_{25} \\ -\frac{1}{2}\Gamma_d\rho_{31} & -\frac{1}{2}(\Gamma_e + \Gamma_d)\rho_{32} & -\Gamma_d\rho_{33} + \Gamma_{r1}\rho_{44} & -\frac{1}{2}(\Gamma_d + \Gamma_{r1})\rho_{34} & -\frac{1}{2}(\Gamma_{\mathrm{d}} + \Gamma_{r2})\rho_{35} \\ -\frac{1}{2}\Gamma_{r1}\rho_{41} & -\frac{1}{2}(\Gamma_e + \Gamma_{r1})\rho_{42} & -\frac{1}{2}(\Gamma_d + \Gamma_{r1})\rho_{43} & -\Gamma_{r1}\rho_{44} & -\frac{1}{2}(\Gamma_{r1} + \Gamma_{r2})\rho_{45} \\ -\frac{1}{2}\Gamma_{r2}\rho_{51} & -\frac{1}{2}(\Gamma_e + \Gamma_{r2})\rho_{52} & -\frac{1}{2}(\Gamma_d + \Gamma_{r2})\rho_{53} & -\frac{1}{2}(\Gamma_{r1} + \Gamma_{r2})\rho_{54} & -\Gamma_{r2}\rho_{55} \end{pmatrix}, \tag{C3}$$

where Ω_p, Ω_d, Ω_c, and $\Omega_{\mathrm{MW}}(t)$ refer to the Rabi frequencies of the probe, dressing, and coupling lasers and the MW field, respectively, which are defined as $\Omega_i = \mu_i E_i/\hbar$. μ_i and E_i are the corresponding dipole moment and the intensity of the electric field. Δ_p, Δ_c, Δ_d, and Δ_{MW}, respectively, present the zero-velocity atom-field detunings of all the above fields. Γ_{r1}, Γ_{r2}, Γ_e, and Γ_d represent the decay rates of the two Rydberg states and two intermediate states, respectively.

In our experiment, we use the MFC field as a strong LO field. The intensity of the MFC field is $E_{\mathrm{MFC}} = \sum_i E_{\mathrm{LO}_i}$, in which E_{LO_i} is the intensity of the ith frequency-comb line. We assume that each of the MFC lines has the same strength $|E_{\mathrm{LO}_1}| = |E_{\mathrm{LO}_2}| = \cdots = |E_{\mathrm{LO}_i}| = |E_{\mathrm{LO}}|$. When the beat note of the signal is small compared with the total LO field power $|E_s| \ll |E_{\mathrm{LO}}|$, we have $2\sum_i |E_{\mathrm{LO}_i}||E_s|\cos(\Delta\omega_i t + \Delta\phi_i) \ll N_L|E_{\mathrm{LO}}|^2$. The total field sensed by the Rydberg atoms is expressed as

$$E_{\mathrm{atom}} \approx \sqrt{N_L}|E_{\mathrm{LO}}|\sqrt{1 + 2\frac{\sum_i |E_s|\cos(\Delta\omega_i t + \Delta\phi_i)}{N_L|E_{\mathrm{LO}}|} + \frac{\sum_{ij}\cos(\Delta\omega_{ij}t + \Delta\phi_{ij})}{N_L}}. \tag{C4}$$

Considering the instant bandwidth of the system and setting the MFC repetition rate (e.g., approximately 4 MHz) larger than the instant bandwidth of the system (approximately 300 kHz), the response of the system to the high-frequency interference terms between different MFC lines $\sum_{ij}^{i\neq j} |E_{\mathrm{LO}_i}||E_{\mathrm{LO}_j}|\cos(\Delta\omega_{ij}t + \Delta\phi_{ij})$ is negligible and the high-order nonlinear response is ignored when E_{LO_i} is not strong (less than -10 dBm). Thus, we consider that the kth MFC line is the nearest neighbor to the signal field:

$$E_{\mathrm{atom}} \approx \sqrt{N_L}|E_{\mathrm{LO}}| + \frac{1}{\sqrt{N_L}}|E_s|\cos(\Delta\omega_k t + \Delta\phi_k). \tag{C5}$$

Thus, the amplitude and phase of the signal are encoded in its beat note with the nearest-neighbor MFC comb line, which is read from the Rydberg nonlinear spectra transmission signal.

In the interaction picture, the detunings $\Delta_1 = \Delta_p$, $\Delta_2 = \Delta_p + \Delta_c$, $\Delta_3 = \Delta_p + \Delta_c + \Delta_d$, and $\Delta_4 = \Delta_p + \Delta_c + \Delta_d - \Delta_{\mathrm{MW}}$. The probe transmission P is expressed as

$$P = P_0 e^{(-2\pi L \mathrm{Im}[\chi]/\lambda_p)}, \tag{C6}$$

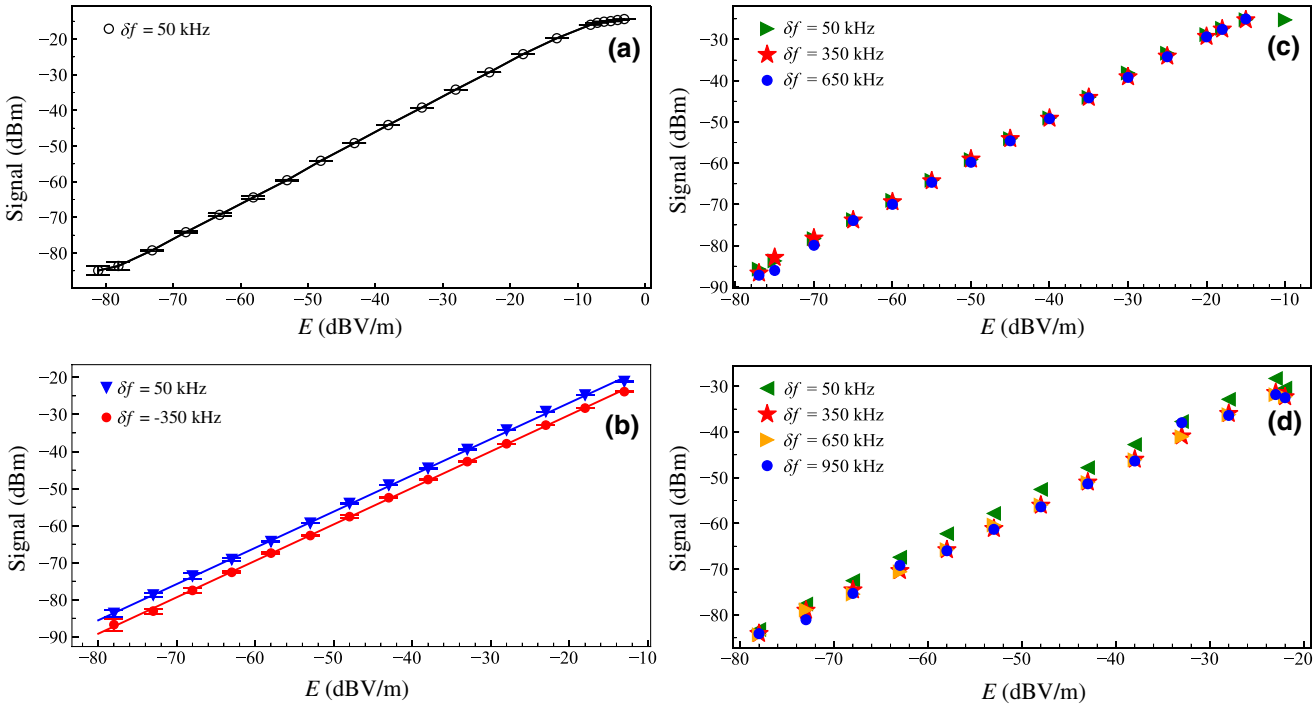

FIG. 8. The measured dynamic range when applying the MFC field with three, five, and seven comb lines. The frequency repetition rate f_r of the MFC is 300 kHz. The frequency offset is set as δf = 50 kHz (green), 350 kHz (red), 650 kHz (orange), and 950 kHz (blue), respectively.

where P_0 is the laser power being input in the vapor cell, χ is the susceptibility of the probe laser $\chi = \frac{2N_0\mathcal{D}_{12}}{E_p\epsilon_0}\rho_{21}$, L is the path of the laser in the cell, N_0 is the total atom density in the vapor cell, μ_{12} is the dipole moment associated with the ground-state transition, E_p denotes the electric field amplitude of the probe laser, and ϵ_0 is the vacuum electric permittivity. For maximum measurement sensitivity, we record the Rydberg MFC spectrum on resonance with the condition $\Delta_p = \Delta_d = \Delta_c = 0$. The instantaneous steady-state solution of the density-matrix element ρ_{21} is calculated through Eq. (C1).

The frequency response curve shown in Fig. 2(a) is modeled through the instant-bandwidth model based on the theory [28,39,40]. We assume that the probe laser is weak and that all the lasers and the MW fields are resonant with the atomic transitions $\Delta_p = \Delta_d = \Delta_c = \Delta_{\mathrm{MW}} = 0$. The atoms are initially populated in the ground state. The reduced optical Bloch equation of the atoms is given based on the first-order perturbation of the probe light. The power (strength) of the beat note against its frequency is calculated through the quasi-steady-state solution of the following equations:

$$\frac{d}{dt}\rho_{21} = -\frac{1}{2}(\Gamma_e + 2\gamma)\rho_{21} + \frac{i}{2}\left(\Omega_p + \Omega_d\rho_{31}\right),$$
$$\frac{d}{dt}\rho_{31} = -\left(2\Gamma_d + 2\gamma\right)\rho_{31} + \frac{i}{2}\left(\Omega_d\rho_{21} + \Omega_c\rho_{41}\right),$$
$$\frac{d}{dt}\rho_{41} = -\frac{1}{2}\left(2\gamma + \Gamma_{r1}\right)\rho_{41} + \frac{i}{2}(\Omega_c\rho_{31} + \Omega_{\mathrm{MW}}(t)\rho_{51}),$$
$$\frac{d}{dt}\rho_{51} = -\frac{1}{2}\left(2\gamma + \Gamma_{r2}\right)\rho_{51} + \frac{i}{2}\Omega_{\mathrm{MW}}(t)\rho_{41}, \qquad \text{(C7)}$$

where the γ represent the transit dephasing rate of the ground state. With $\gamma \gg \Gamma_{r1}, \Gamma_{r2}$, these two decay rates for the Rydberg states are not considered in the calculation. This transient pattern (the instant bandwidth) is independent of the LO frequency. The experimental frequency response data show good agreement with our bandwidth-model calculation (black solid line) in Fig. 2(a). Also, the curve fits well with an exponential decay function. We use a scaling factor in our theory curves that only considers the relative intensity of the beat note, as we set the maximum signal amplitude as a reference point.

APPENDIX D: DYNAMIC RANGE VARIATION WITH THE NUMBER OF MFC LINES

The sensitivity of the system is dependent on the number of MFC comb lines and the power of the MFC field. We plot the power of the detected beat note versus the E-field intensity of the applied signal when using a single LO field in Fig. 8(a) for comparison. Figure 8(b) shows the beat-note response when using a MFC field with three comb lines and a repetition rate of $f_r = 300$ kHz. We want

to emphasize that the dynamic range is affected by the relative phase of each line of the MFC. There is a difference for a dynamic range of approximately 8 dB (from 65 dB to 57 dB) between the MFC with optimized phase and the one without optimization. The optimized phase of the frequency lines is set as 0, 0, and π. We only plot input signals that have frequency offsets δf of 50 kHz, 350 kHz from the center frequency (f_{LO}= 4.485 GHz). To compare the response within the range covered by different comb lines, the beat-note frequencies are all 50 kHz. Figure 8(c) [Fig. 8(d)] shows the response when the MFC with five (seven) comb lines is set as LO and the average dynamic range is 62.8 dB (56 dB). According to Eq. (1), the beat-note response decreases with an increase in the number of MFC lines.

[1] T. W. Hänsch, Nobel lecture: Passion for precision, Rev. Mod. Phys. **78**, 1297 (2006).

[2] N. Picqué and T. W. Hänsch, Frequency comb spectroscopy, Nat. Photonics **13**, 146 (2019).

[3] L.-S. Ma, Z. Bi, A. Bartels, L. Robertsson, M. Zucco, R. S. Windeler, G. Wilpers, C. Oates, L. Hollberg, and S. A. Diddams, Optical frequency synthesis and comparison with uncertainty at the 10–19 level, Science **303**, 1843 (2004).

[4] A. D. Ludlow, M. M. Boyd, J. Ye, E. Peik, and P. O. Schmidt, Optical atomic clocks, Rev. Mod. Phys. **87**, 637 (2015).

[5] A. Rueda, F. Sedlmeir, M. Kumari, G. Leuchs, and H. G. Schwefel, Resonant electro-optic frequency comb, Nature **568**, 378 (2019).

[6] E. Lucas, P. Brochard, R. Bouchand, S. Schilt, T. Südmeyer, and T. J. Kippenberg, Ultralow-noise photonic microwave synthesis using a soliton microcomb-based transfer oscillator, Nat. Commun. **11**, 1 (2020).

[7] R. P. Erickson, M. R. Vissers, M. Sandberg, S. R. Jefferts, and D. P. Pappas, Frequency Comb Generation in Superconducting Resonators, Phys. Rev. Lett. **113**, 187002 (2014).

[8] P. Lu, T.-C. Chien, X. Cao, O. Lanes, C. Zhou, M. J. Hatridge, S. Khan, and H. E. Türeci, Nearly Quantum-Limited Josephson-Junction Frequency-Comb Synthesizer, Phys. Rev. Appl. **15**, 044031 (2021).

[9] S.-C. Chan, G.-Q. Xia, and J.-M. Liu, Optical generation of a precise microwave frequency comb by harmonic frequency locking, Opt. Lett. **32**, 1917 (2007).

[10] Y.-S. Juan and F.-Y. Lin, Ultra broadband microwave frequency combs generated by an optical pulse-injected semiconductor laser, Opt. Express **17**, 18596 (2009).

[11] Y. Hu, S. Ding, Y. Qin, J. Gu, W. Wan, M. Xiao, and X. Jiang, Generation of Optical Frequency Comb via Giant Optomechanical Oscillation, Phys. Rev. Lett. **127**, 134301 (2021).

[12] G. Dousmanis, T. Sanders, Jr., and C. Townes, Microwave spectra of the free radicals OH and OD, Phys. Rev. **100**, 1735 (1955).

[13] E. Hirota, *High-Resolution Spectroscopy of Transient Molecules* (Springer Berlin, Heidelberg, 2012), Vol. 40.

[14] M. Saffman, T. G. Walker, and K. Mølmer, Quantum information with Rydberg atoms, Rev. Mod. Phys. **82**, 2313 (2010).

[15] A. K. Mohapatra, M. G. Bason, B. Butscher, K. J. Weatherill, and C. S. Adams, A giant electro-optic effect using polarizable dark states, Nat. Phys. **4**, 890 (2008).

[16] H. Fan, S. Kumar, J. Sedlacek, H. Kübler, S. Karimkashi, and J. P. Shaffer, Atom based rf electric field sensing, J. Phys. B **48**, 202001 (2015).

[17] J. A. Sedlacek, A. Schwettmann, H. Kübler, R. Löw, T. Pfau, and J. P. Shaffer, Microwave electrometry with Rydberg atoms in a vapour cell using bright atomic resonances, Nat. Phys. **8**, 819 (2012).

[18] A. Facon, E.-K. Dietsche, D. Grosso, S. Haroche, J.-M. Raimond, M. Brune, and S. Gleyzes, A sensitive electrometer based on a Rydberg atom in a Schrödinger-cat state, Nature **535**, 262 (2016).

[19] M. Jing, Y. Hu, J. Ma, H. Zhang, L. Zhang, L. Xiao, and S. Jia, Atomic superheterodyne receiver based on microwave-dressed Rydberg spectroscopy, Nat. Phys. **16**, 911 (2020).

[20] M. T. Simons, A. H. Haddab, J. A. Gordon, and C. L. Holloway, A Rydberg atom-based mixer: Measuring the phase of a radio frequency wave, Appl. Phys. Lett. **114**, 114101 (2019).

[21] A. K. Robinson, N. Prajapati, D. Senic, M. T. Simons, and C. L. Holloway, Determining the angle-of-arrival of a radio-frequency source with a Rydberg atom-based sensor, Appl. Phys. Lett. **118**, 114001 (2021).

[22] K. C. Cox, D. H. Meyer, F. K. Fatemi, and P. D. Kunz, Quantum-Limited Atomic Receiver in the Electrically Small Regime, Phys. Rev. Lett. **121**, 110502 (2018).

[23] H. Q. Fan, S. Kumar, R. Daschner, H. Kübler, and J. P. Shaffer, Subwavelength microwave electric-field imaging using Rydberg atoms inside atomic vapor cells, Opt. Lett. **39**, 3030 (2014).

[24] D. H. Meyer, P. D. Kunz, and K. C. Cox, Waveguide-Coupled Rydberg Spectrum Analyzer from 0 to 20 GHz, Phys. Rev. Appl. **15**, 014053 (2021).

[25] Z.-K. Liu, L.-H. Zhang, B. Liu, Z.-Y. Zhang, G.-C. Guo, D.-S. Ding, and B.-S. Shi, Deep learning enhanced Rydberg multifrequency microwave recognition, Nat. Commun. **13**, 1997 (2022).

[26] Z.-C. Shi, Y.-H. Chen, W. Qin, Y. Xia, X. X. Yi, S.-B. Zheng, and F. Nori, Two-level systems with periodic *n*-step driving fields: Exact dynamics and quantum state manipulations, Phys. Rev. A **104**, 053101 (2021).

[27] L.-S. Ma, M. Zucco, S. Picard, L. Robertsson, and R. Windeler, A new method to determine the absolute mode number of a mode-locked femtosecond-laser comb used for absolute optical frequency measurements, IEEE J. Sel. Top. Quantum **9**, 1066 (2003).

[28] D. H. Meyer, K. C. Cox, F. K. Fatemi, and P. D. Kunz, Digital communication with Rydberg atoms and amplitude-modulated microwave fields, Appl. Phys. Lett. **112**, 211108 (2018).

[29] C. Carr, M. Tanasittikosol, A. Sargsyan, D. Sarkisyan, C. S. Adams, and K. J. Weatherill, Three-photon electromagnetically induced transparency using Rydberg states, Opt. Lett. **37**, 3858 (2012).

[30] N. Thaicharoen, K. R. Moore, D. A. Anderson, R. C. Powel, E. Peterson, and G. Raithel, Electromagnetically induced transparency, absorption, and microwave-field sensing in a Rb vapor cell with a three-color all-infrared laser system, Phys. Rev. A **100**, 063427 (2019).

[31] A. Osterwalder and F. Merkt, Using High Rydberg States as Electric Field Sensors, Phys. Rev. Lett. **82**, 1831 (1999).

[32] A. K. Mohapatra, T. R. Jackson, and C. S. Adams, Coherent Optical Detection of Highly Excited Rydberg States Using Electromagnetically Induced Transparency, Phys. Rev. Lett. **98**, 113003 (2007).

[33] J. Meinel, V. Vorobyov, B. Yavkin, D. Dasari, H. Sumiya, S. Onoda, J. Isoya, and J. Wrachtrup, Heterodyne sensing of microwaves with a quantum sensor, Nat. Commun. **12**, 1 (2021).

[34] M. G. Bason, M. Tanasittikosol, A. Sargsyan, A. K. Mohapatra, D. Sarkisyan, R. M. Potvliege, and C. S. Adams, Enhanced electric field sensitivity of rf-dressed Rydberg dark states, New J. Phys. **12**, 065015 (2010).

[35] L. A. Downes, A. R. MacKellar, D. J. Whiting, C. Bourgenot, C. S. Adams, and K. J. Weatherill, Full-field terahertz imaging at kilohertz frame rates using atomic vapor, Phys. Rev. X **10**, 011027 (2020).

[36] S. Chen, D. J. Reed, A. R. MacKellar, L. A. Downes, N. F. A. Almuhawish, M. J. Jamieson, C. S. Adams, and K. J. Weatherill, Terahertz electrometry via infrared spectroscopy of atomic vapor, Optica **9**, 485 (2022).

[37] S. Bartalini, L. Consolino, P. Cancio, P. De Natale, P. Bartolini, A. Taschin, M. De Pas, H. Beere, D. Ritchie, M. S. Vitiello, and R. Torre, Frequency-comb-assisted terahertz quantum cascade laser spectroscopy, Phys. Rev. X **4**, 021006 (2014).

[38] T. Yasui, Y. Kabetani, E. Saneyoshi, S. Yokoyama, and T. Araki, Terahertz frequency comb by multifrequency-heterodyning photoconductive detection for high-accuracy, high-resolution terahertz spectroscopy, Appl. Phys. Lett. **88**, 241104 (2006).

[39] Y.-F. Chen, G.-C. Pan, and I. A. Yu, Transient behaviors of photon switching by quantum interference, Phys. Rev. A **69**, 063801 (2004).

[40] G. Dmochowski, A. Feizpour, M. Hallaji, C. Zhuang, A. Hayat, and A. M. Steinberg, Experimental Demonstration of the Effectiveness of Electromagnetically Induced Transparency for Enhancing Cross-Phase Modulation in the Short-Pulse Regime, Phys. Rev. Lett. **116**, 173002 (2016).